Published in final edited form as:
Magn Reson Med. 2015 March ; 73(3): 1026–1033. doi:10.1002/mrm.25216.

Noncontrast Peripheral MRA with Spiral Echo Train Imaging

Samuel W. Fielden[1], **John P. Mugler III**[1,2], **Klaus D. Hagspiel**[2], **Patrick T. Norton**[2], **Christopher M. Kramer**[2,3], and **Craig H. Meyer**[1,2,*]

[1]Department of Biomedical Engineering, University of Virginia, Charlottesville, Virginia, USA

[2]Department of Radiology and Medical Imaging, University of Virginia, Charlottesville, Virginia, USA

[3]Department of Medicine, University of Virginia, Charlottesville, Virginia, USA

Abstract

Purpose—To develop a spin echo train sequence with spiral readout gradients with improved artery–vein contrast for noncontrast angiography.

Theory—Venous T_2 becomes shorter as the echo spacing is increased in echo train sequences, improving contrast. Spiral acquisitions, due to their data collection efficiency, facilitate long echo spacings without increasing scan times.

Methods—Bloch equation simulations were performed to determine optimal sequence parameters, and the sequence was applied in five volunteers. In two volunteers, the sequence was performed with a range of echo times and echo spacings to compare with the theoretical contrast behavior. A Cartesian version of the sequence was used to compare contrast appearance with the spiral sequence. Additionally, spiral parallel imaging was optionally used to improve image resolution.

Results—In vivo, artery–vein contrast properties followed the general shape predicted by simulations, and good results were obtained in all stations. Compared with a Cartesian implementation, the spiral sequence had superior artery–vein contrast, better spatial resolution (1.2 mm^2 versus 1.5 mm^2), and was acquired in less time (1.4 min versus 7.5 min).

Conclusion—The spiral spin echo train sequence can be used for flow-independent angiography to generate threedimensional angiograms of the periphery quickly and without the use of contrast agents.

Keywords

noncontrast angiography; peripheral angiography; flow-independent angiography

*Correspondence to: Craig H. Meyer, Ph.D., Department of Biomedical Engineering, University of Virginia, Box 800759, Charlottesville, VA 22908. cmeyer@virginia.edu.

INTRODUCTION

Peripheral arterial disease is a common disease of the lower-limb vasculature that is associated with a greater risk for renal and coronary vascular disease. Clinically, MR angiography (MRA) has been used to diagnose and monitor luminal obstruction because, in contrast to computed tomography angiography, it does not expose the patient to ionizing radiation and is minimally invasive. The current gold-standard for MRA is contrast-enhanced MRA (1,2); however, the established link between gadolinium-based contrast agents and nephrogenic systemic fibrosis (3,4) in at-risk patients has led to renewed interest in developing noncontrast MRA techniques.

In general, noncontrast MRA techniques fall into two categories: flow-dependent and flow-independent. Early noncontrast MRA techniques such as time-of-flight (5) and phase contrast angiography (6) generate contrast by exploiting the fact that blood is moving relative to surrounding, stationary background signal. Some examples of newer techniques that fall into the flow-dependent category are the promising QISS technique (7), in which an inversion pulse is used to improve background suppression, and the popular fresh-blood imaging methods that combine flow-spoiled systolic- and diastolic-phase acquisitions to generate bright-artery contrast (8,9). For all flow-dependent methods, the inherent risk is that, in regions of slow or retrograde flow, arterial contrast may be reduced in just the regions that are of most interest (i.e., around the stenosis). Additionally, many of these methods must be tailored to each patient and each station, as the sequence parameters must be adjusted depending on blood flow rate.

Flow-independent angiography, on the other hand, uses the intrinsic tissue properties of blood to generate contrast, rather than relying on the fact that it is flowing (8–11). As such, regions of slow, in-plane, and retrograde flow often found in patients may be imaged; however, sufficient background and venous suppression can be challenging when using these methods.

The recent sequences used for flow-independent angiography have mostly been variations on magnetization-prepared balanced steady state free precession (bSSFP; also known as TrueFISP, FIESTA, or b-FFE) due to its efficiency in generating bright blood contrast. Blood has a long T_1 and a variable T_2, depending on its oxygenation status (12); blood-muscle and arterial-venous contrast may therefore be obtained by straightforward T_2-weighting of the images. Since their introduction, turbo spin echo (TSE) sequences have become workhorses for clinical T_2-weighted imaging; however, conventional TSE sequences are susceptible to flow-related artifacts and signal loss, and this sensitivity to flow makes these sequences unsuitable for applications involving flowing spins without modifications to reduce flow sensitivity (13).

This work builds on our previous experience with using TSE sequences for noncontrast angiography with two important modifications: First, we use spiral readouts here. Moving to spiral readouts has three main advantages over Cartesian scanning in peripheral MRA: (i) The natural motion insensitivity of spiral gradients is attractive for a sequence wherein we wish to remove artifacts due to flow; (ii) Spiral gradients will allow for longer echo

spacings, improving venous suppression according to the Luz-Meiboom model; and (iii) More efficient coverage of k-space will lead to less power deposition to the patient. The rapid coverage of k-space by spiral scanning has been used for many years in applications such as coronary artery imaging where scanning must be conducted quickly and with minimal motion and flow artifacts (10).

Second, the sequence described in (13) was a fully refocused TSE sequence that shares many characteristics with a bSSFP sequence, including an unfortunate sensitivity to B_1 inhomogeneity, the result of which was insufficient fat suppression. In cases where the majority of flow is in one known direction, such as in the leg, the net gradient moments can be placed such that they do not affect the majority of flowing spins. Here, we return to an unbalanced, traditional TSE sequence, but ensure flow-spoiling occurs in the least objectionable direction by placing crusher gradients in the through-plane (anterior–posterior) direction of the imaging volume.

THEORY

In flow-independent angiography, bright-blood contrast is obtained primarily by means of T_2 weighting of the images, either through a T_2-prep module (10,11,14) or by acquiring late echoes in a spin-echo sequence (13,15). Blood has a longer T_2 than most of the tissues surrounding it in the periphery, but this T_2 is dependent on its oxygenation status and on how often refocusing pulses are applied in the spin-echo train.

Red blood cells constitute a separate compartment from the surrounding plasma. Within a red blood cell, the magnetic microenvironment is governed by the extent to which hemoglobin is oxygenated, as deoxyhemoglobin is paramagnetic. As water molecules are freely exchanged between the two blood compartments, protons are exposed to the variable magnetic microenvironment present within red blood cells, leading to dephasing. Blood's dependence on the rate at which refocusing pulses are applied is therefore due to the varying amounts of time protons are resident in either compartment before they experience the next refocusing pulse. The Luz-Meiboom model may be used to model T_2 relaxation in the presence of two-site exchange and under rapid refocusing conditions, as occurs during a TSE echo train (12,16):

$$\frac{1}{\mathrm{T2_b}}=\frac{1}{\mathrm{T2_o}}+(\mathrm{P_A})(1-\mathrm{P_A})\tau_{\mathrm{ex}}\left[\left(1-\frac{\%\mathrm{HbO_2}}{100\%}\right)\alpha\omega_0\right]^2\times\left(1-\frac{2\tau_{\mathrm{ex}}}{\tau_{180}}\tanh\frac{\tau_{180}}{2\tau_{\mathrm{ex}}}\right) \quad [1]$$

where $T2_b$ is the T_2 of blood, $T2_o$ is the T_2 of fully oxygenated blood, P_A is the fraction of protons resident in one site, τ_{ex} is a measure of the average time required for a proton to move between the two sites, % HbO_2 is the percent oxygenation of blood, α is a dimensionless value related to the susceptibility of deoxyhemoglobin and the geometry of the red blood cell, ω_0 is the resonant proton frequency, and τ^{180} is the echo spacing between refocusing pulses in the echo train. This equation states that, as the percent oxygenation goes down or the echo spacing of the refocusing pulses increases, the apparent T_2 of blood becomes shorter. This means that effective T_2 contrast can be generated between arteries and veins during a spin echo train with sufficiently long echo spacings between RF pulses. Figure 1 plots the blood signal acquired at a echo time (TE) of 130 ms for various

oxygenation states and echo spacings using the Luz-Meiboom equation to estimate blood T_2 in a spin echo train sequence.

A volumetric TSE sequence with a long TE necessarily has an extremely long echo train duration (several hundred milliseconds). Simply increasing the echo spacing in this sequence would push the echo train duration past the usable limit, as determined by arterial T_2, reducing image quality. A second option would be to adopt k-space segmentation methods, increasing scan times. Spiral readout gradients offer improved acquisition efficiency and provide a path to achieving long echo spacings while maintaining reasonable scan times.

In previous work using refocused spin echo trains for flow-independent angiography, adequate fat suppression proved very difficult to achieve. Due to fat's rapid T_1 recovery and in the presence of B_1 inhomogeneity, free induction decays (FIDs) are generated off of each refocusing radiofrequency (RF) pulse no matter what fat suppression technique is performed at the beginning of the echo train. The use of so-called crusher gradients dephases the signal arising from these FID components, allowing pure T_2 contrast to prevail as the signal evolves along the echo train. For this reason, the sequence used in this work includes crusher gradients in the throughplane (anterior–posterior) direction, which is justified because there is relatively little flow in that direction in the peripheral vasculature. This approach along with fat suppression before the excitation pulse yields very good fat suppression while maintaining insensitivity to inplane (coronal) flow.

METHODS

Here, a three-dimensional (3D) stack-of-spirals trajectory was used, with each partition collected at a different TE within a spin echo train. The trajectory consists of a parallel stack of 2D spiral disks, with phase encoding along the third dimension, such that the volume covered in kspace is a cylinder (Fig. 2). This permits off-resonance correction by executing 2D off-resonance correction slice-by-slice in 3D (17).

To take full advantage of the available time and improve acquisition efficiency, the spiral readout is centered in the 180° interpulse period (Fig. 2). Accordingly, the spin-echo forms midway through the readout and is placed at some radius in k-space, rather than at the center, as in conventional TSE. In our experience, this has no effect on image quality or contrast for long-TE imaging.

To identify optimal sequence timing parameters, Bloch equation simulations were performed to assess signal evolutions for arterial and venous blood during a TSE echo train with different echo spacings (Fig. 3). The variable relaxation rate of blood was modeled using the Luz-Meiboom model as described in (12) to estimate blood T_2 during a spin echo train. Other simulation parameters were: $T_{1,blood}$ = 1900 ms, $T_{2,oxygenated\ blood}$ = 275 ms (18), B_0 = 3T, echo train duration = 600 ms, arterial oxygenation = 95%, venous oxygenation = 60%, hematocrit = 40%, P = 36%, τ = 3 ms, α = 0.7 ppm, refocusing flip angle = 180°. The simulations show that as the spacing between refocusing pulses is

increased, the maximum artery–vein contrast increases and, furthermore, the maximum contrast occurs earlier in the echo train.

A target echo spacing of 10 ms was chosen based on the fact that echo spacings above ~10 ms yield progressively smaller gains in contrast (Fig. 1) coupled with the knowledge that long spiral readout durations promote image blurring. A spiral readout duration of 6.4 ms within a 10 ms interpulse period resulted in good artery–vein contrast and acceptable image sharpness. The remaining interpulse time is dedicated to through-plane crusher gradients and to the spiral rewinder gradients.

3D Reordering and Partial k-Space

Each echo train in the sequence collects one interleaf from each partition in the acquisition volume in a linear manner. Partial k-space coverage techniques have been used extensively in spin-echo train imaging (19), and they are prevalent in the TSE sequences used for flow-spoiled fresh-blood imaging (20). These techniques exploit the conjugate symmetry property of k-space and only acquire ~50–90% of the data required to completely fill k-space. The missing data are then filled in before reconstruction takes place. Here, partial k-space coverage can be performed in the 3D phase-encoding direction to reduce the number of phase encodes that need to be performed, shortening echo train lengths (which are necessarily quite long). The sequence automatically performs a partial k-space acquisition depending on the effective echo time chosen by the user. For echo times typically used in this work, this results in partial k-space factors of approximately 0–30% (i.e., 70–100% of the data is acquired). Missing partitions are filled in after gridding using a homodyne partial-Fourier reconstruction algorithm.

Parallel Imaging

A small amount of spiral undersampling is typically used to improve image resolution. We have implemented in-plane (non-Cartesian) parallel imaging by means of the SPIRiT reconstruction algorithm available from Dr. Michael Lustig (21), which uses the fully sampled center of k-space from a dual-density spiral k-space trajectory to calibrate the reconstruction. SPIRiT reconstruction takes place slice-by-slice after a 1D Fourier transform in the through-plane direction, and is followed by a semiautomatic off-resonance correction step (22,23). As mentioned previously, there are usually some missing partitions due to partial k-space acquisition. In this case, the SPIRiT reconstruction is applied within the homodyne algorithm. In the abdominal and thigh stations, relatively modest resolutions of around 1.2 mm^2 require no acceleration. In the calf station, the resolution requirement is a bit higher, and here modest in-plane undersampling factors of 2–4 are used to keep scan times reasonably short.

Fluid Suppression

An inversion pulse can be applied before excitation to null long-T_2 extracellular fluid (synovial fluid and edema) signal based on its unique T_1. This should be evaluated on a case-by-case basis, however, because the application of an inversion pulse will have a deleterious effect on other signals as well. In this proof-of-principle study, optimization of artery–vein contrast with respect to inversion time (TI) and TR was not performed. Instead,

TR was increased to 10 s, and TI was set to 2500 ms, based on fluid's T_1 value of approximately 3600 ms at 3T.

In Vivo Experiments

All scans were performed on a Siemens 3.0 Tesla (T) Trio scanner (Siemens Healthcare) with peripheral MRA coils placed anteriorly and laterally and a spine coil placed posteriorly. The protocol was approved by the Institutional Review Board at our university and all participants gave written informed consent. Subjects were scanned in the supine position, with the stack-of-spirals volume oriented coronally (i.e., the through-plane direction was anterior–posterior). To avoid spiral artifacts arising from signal outside of the imaging volume, MRA and spine coils were turned on only for the station being acquired; that is, the coil volume was completely circumscribed by the coronally oriented spiral field of view (FOV). All scans began with the acquisition of a low-resolution 3D field map for off-resonance correction, and spiral data were reconstructed onto a 512 × 512 matrix.

Two male volunteers (ages 25 and 27) were scanned with variations of the spiral TSE sequence to demonstrate its artery–vein contrast properties. First, a constant echo spacing of 10 ms was used with the TE varied between 55 and 325 ms, number of interleaves = 25 to achieve an in-plane resolution of 1.2 mm^2 over a 400 mm^2 FOV, TR = 3 s, refocusing flip angle = 180°, with all excitation and refocusing pulses nonselective. Through-plane resolution was 2 mm with 64 3D phase encodes. Both chemical-shift-selective fat suppression as well as a STIR (short TI inversion recovery) pulse were used for fat suppression. No parallel-imaging acceleration was used for these scans. The total echo train duration varied depending on TE, but typically fell in a range between 300 and 600 ms. Total scan time was 1.4 min per image volume.

Next, echo spacing was varied between 6.2 and 11.8 ms with a constant TE of 165 ms. For this experiment, increasing echo spacing in the sequence automatically results in longer readout events, so the total number of spiral interleaves was adjusted to maintain a constant 1.2 mm^2 in-plane resolution.

Additionally, one volunteer was scanned with a Cartesian version of the sequence with echo spacing = 3.8 ms for comparison. The optimal TE predicted for this echo spacing is around 230 ms. Due to specific energy absorption rate (SAR) limits, the Cartesian sequence was acquired with 1.5 mm^3 isotropic resolution and TR = 4720 ms. The resulting scan time was 7.5 min.

For each image set, three reformatted slices at different locations in the leg were used to measure femoral arterial and venous signals to determine artery–vein contrast. All intensities were measured using the mean signal from ovoid regions of interest in axial reformats from the 3D volumetric data.

Two additional scans were performed. First, the utility of a FLAIR (fluid attenuated inversion recovery) pulse to remove synovial fluid was demonstrated in one volunteer by adding a nonselective inversion recovery pulse with TI 2500 ms (TR was increased to 10 s). Second, the thigh and calf stations of 3 volunteers (ages, 28–29 years) were scanned using

the optimized parameters described above. For the thigh, echo spacing = 10 ms, TR/TE = 3000/130 ms, number of interleaves was 25 to achieve an in-plane resolution of 1.2 mm^2 over a 400 mm^2 FOV, refocusing flip angle = 180°, with all excitation and refocusing pulses nonselective. Through-plane resolution was 2 mm with 64 3D phase encodes. Both chemical-shift-selective fat suppression as well as a STIR pulse were used for fat suppression. No parallel-imaging acceleration was used for these scans. Total scan time was 1.4 min per image volume. For the calf, all parameters were the same, except that the parallel-imaging acceleration factor was increased to a modest value of 2, resulting in an in-plane resolution of 1.0 mm^2.

RESULTS

Figure 4 shows that, for a 10 ms echo spacing in normal volunteers, artery–vein contrast peaks around 100 ms. Furthermore, any TE over approximately 80 ms is very effective at suppressing background muscle. Early TEs are advantageous in that they result in more signal being deposited near the center of k-space before T_2 decay removes available magnetization. The reduction in signal-to-noise ratio (SNR) due to a late TE is especially apparent in the TE = 325 ms image.

As predicted by the Luz-Meiboom model, larger echo spacings within the echo train result in better venous suppression (Fig. 5). By moving from an echo spacing of 3.8 ms in a Cartesian sequence to 10 ms using a spiral sequence, the contrast-to-noise ratio (CNR) between arteries and veins is improved by 235% (Fig. 6). Furthermore, despite the drastically reduced scan time (1.4 min for spiral; 7.5 min for Cartesian), it is clear in Figure 6 that the increased efficiency of spiral readout gradients results in better in-plane resolution over its Cartesian counterpart (1.2 mm^2 versus 1.5 mm^2).

Figure 7 demonstrates that synovial fluid in the knee can be effectively removed with the application of an inversion pulse with TI 2500 ms (TR must be increased accordingly). However, this dramatically increases scan time and has a deleterious effect on other signals.

As a final example, Figure 8 shows maximum intensity projections (MIPs) of the thigh and calf stations of three volunteers, displaying excellent artery–muscle and artery–vein contrast.

DISCUSSION

In the spiral TSE sequence, signal from flow is maintained by ensuring the net area of the in-plane spiral gradients is zero within each echo spacing. In contrast to flow-spoiled methods which also use the TSE sequence and must be tailored to each patient and each station, contrast between arteries and surrounding tissues is generated here by T_2 differences, and in particular, artery–vein contrast is obtained without the use of gated, subtracted acquisitions but rather by manipulating the effective T_2 of venous blood through extended echo spacings. This is a novel contrast generation method for peripheral angiography in the context of TSE sequences.

Because flow-independent angiography is sensitive to changes in blood oxygenation, it is expected that the optimal TE for artery–vein contrast will need to be adjusted to an earlier

time in the echo train for clinical imaging. In light of this and by studying Figure 3, a potential disadvantage of long echo spacings is apparent: longer echo spacings result in more “peaky” contrast curves. For patients, who present with a wide range of venous oxygenation states, missing the optimal TE becomes more likely and more costly in terms of contrast generation. In this case, prescans may be necessary to determine optimal sequence parameters based on blood oxygenation levels. Furthermore, the wide range of venous oxygenations states presented by patients is a potential concern when using any T_2-weighted noncontrast MRA method, as lower oxygenation extraction in the extremities will result in poorer artery–vein differentiation. Further exploration of this sequence in patients is necessary to determine its clinical utility.

In contrast to Cartesian trajectories, spiral trajectories much more efficiently cover k-space for data acquisition (24). Additionally, the gradient moments associated with spiral imaging are small and are easily nulled with careful rewinder design. This, along with speedy acquisition times, makes spiral imaging resistant to flow-related artifacts (25). Spiral readouts are therefore an appropriate choice for this application because they are excellent candidates for a sequence wherein blood motion must not impact image formation. Simply increasing the echo spacing in a Cartesian TSE sequence would push echo train lengths to untenable durations, necessitating the use of segmented acquisitions, and would therefore have a negative impact on scan time. The efficiency of spirals means that extended echo spacings can be achieved while maintaining reasonable scan times. In fact, the scan time using the 3D spiral TSE sequence in the example included here was over 5.3 times faster than the scan time required using its Cartesian counterpart.

A second advantage related to the efficiency of spiral readouts for this sequence is reduced power deposition to the subject. In a Cartesian sequence, the design of the k-space reordering method along with the short echo spacing dictates several hundred 180° refocusing pulses be played out in a single echo train, or else k-space segmentation methods must be used. It is very common to either have to reduce the refocusing flip angle or extend TR to satisfy SAR limits when using long echo train duration TSE sequences. Because the spiral sequence traverses k-space differently—and with much larger echo spacings—the number of RF pulses played out during a single echo train is much lower, and SAR limits are rarely encountered.

Because the through-plane direction is traversed *within* an echo train as the 3D phase encoding direction in this sequence, aberrant signal evolutions caused by improper k-space reordering will have the greatest impact in this direction. For angiography, where we desire strong T_2 weighting, long TEs allow the use of a linear reordering scheme, which is conceptually and physically the simplest option available. For other applications of the spiral TSE sequence, however, where an early TE is desired for SNR or contrast properties, other reordering schemes may be used. In these cases, careful design of the k-space reordering scheme will be necessary.

The crusher gradients used in this sequence are placed in the anterior–posterior direction, and therefore did not appear to impact flowing blood signal in normal volunteers. However,

there exists a potential loss of signal for vessels oriented along the crusher-gradient axis, as may be the case for the tortuous collateral vessels often seen in patients.

The inclusion of parallel imaging, as shown in the calf station of Figure 8, is optional when using this method; the technique is still rapid without using it. In the future, parallel imaging may prove to be more important for applications in the abdomen and thorax, where cardiac and respiratory motion require a more demanding acquisition protocol.

In conclusion, the spiral TSE sequence is capable of using flow-independent angiography to generate 3D angiograms of the periphery quickly and without the use of contrast agents. The sequence is faster, has less SAR, and results in better contrast than its Cartesian counterpart.

ACKNOWLEDGMENT

S.W.F. received an American Heart Association Predoctoral Fellowship.

Grant sponsor: National Institutes of Health; Grant numbers: R01 HL079110, R01 HL075792, T32 HL007284; Grant sponsor: Siemens Medical Solutions.

REFERENCES

1. Lakshminarayan R, Simpson JO, Ettles DF. Magnetic resonance angiography: current status in the planning and follow-up of endovascular treatment in lower-limb arterial disease. Cardiovasc Intervent Radiol. 2009; 32:397–405. [PubMed: 19130124]
2. Hadizadeh DR, Gieseke J, Lohmaier SH, Wilhelm K, Boschewitz J, Verrel F, Schild HH, Willinek WA. Peripheral MR angiography with blood pool contrast agent: prospective intraindividual comparative study of high-spatial-resolution steady-state MR angiography versus standard-resolution first-pass MR angiography and DSA. Radiology. 2008; 249:701–711. [PubMed: 18769017]
3. Thomsen HS. Nephrogenic systemic fibrosis: a serious late adverse reaction to gadodiamide. Eur Radiol. 2006; 16:2619–2621. [PubMed: 17061066]
4. Weinreb JC, Abu-Alfa AK. Gadolinium-based contrast agents and nephrogenic systemic fibrosis: why did it happen and what have we learned? J Magn Reson Imaging. 2009; 30:1236–1239. [PubMed: 19938035]
5. Steinberg FL, Yucel EK, Dumoulin CL, Souza SP. Peripheral vascular and abdominal applications of MR flow imaging techniques. Magn Reson Med. 1990; 14:315–320. [PubMed: 2345511]
6. Reimer P, Boos M. Phase-contrast MR angiography of peripheral arteries: technique and clinical application. Eur Radiol. 1999; 9:122–127. [PubMed: 9933395]
7. Edelman RR, Sheehan JJ, Dunkle E, Schindler N, Carr J, Koktzoglou I. Quiescent-interval single-shot unenhanced magnetic resonance angiography of peripheral vascular disease: technical considerations and clinical feasibility. Magn Reson Med. 2010; 63:951–958. [PubMed: 20373396]
8. Wright GA, Nishimura DG, Macovski A. Flow-independent magnetic resonance projection angiography. Magn Reson Med. 1991; 17:126–140. [PubMed: 2067389]
9. Brittain JH, Olcott EW, Szuba A, Gold GE, Wright GA, Irarrazaval P, Nishimura DG. Three-dimensional flow-independent peripheral angiography. Magn Reson Med. 1997; 38:343–354. [PubMed: 9339435]
10. Brittain JH, Hu BS, Wright GA, Meyer CH, Macovski A, Nishimura DG. Coronary angiography with magnetization-prepared T2 contrast. Magn Reson Med. 1995; 33:689–696. [PubMed: 7596274]
11. Cukur T, Lee JH, Bangerter NK, Hargreaves BA, Nishimura DG. Non-contrast-enhanced flow-independent peripheral MR angiography with balanced SSFP. Magn Reson Med. 2009; 61:1533–1539. [PubMed: 19365850]

12. Wright GA, Hu BS, Macovski A. Estimating oxygen saturation of blood in vivo with MR imaging at 1.5 T. J Magn Reson Imaging. 1991; 1:275–283. [PubMed: 1802140]
13. Fielden SW, Mugler JP, Hagspiel KD, Norton PT, Kramer CM, Meyer CH. Refocused turbo spin-echo for noncontrast peripheral MR angiography. J Magn Reson Imaging. 2013
14. Cukur T, Shimakawa A, Yu H, Hargreaves BA, Hu BS, Nishimura DG, Brittain JH. Magnetization-prepared IDEAL bSSFP: a flow-independent technique for noncontrast-enhanced peripheral angiography. J Magn Reson Imaging. 2011; 33:931–939. [PubMed: 21448960]
15. Fielden, SW.; Tan, H.; Mugler, JP.; Kramer, CM.; Meyer, CH. Noncontrast MRA using spiral refocused turbo spin echo. In Proceedings of the Joint Annual Meeting of ISMRM-ESMRMB; Stockholm, Sweden. 2010. Abstract 3788.
16. Luz Z, Meiboom S. Nuclear magnetic resonance study of the protolysis of trimethylammonium ion in aqueous solution—order of the reaction with respect to solvent. J Chem Phys. 1963; 39:366–370.
17. Chen, W.; Meyer, CH. Off-resonance correction for 3D imaging using a stack of spirals trajectory. In Proceedings of the 14th Annual Meeting of ISMRM; Seattle, Washington, USA. 2006. Abstract 2966.
18. Stanisz GJ, Odrobina EE, Pun J, Escaravage M, Graham SJ, Bronskill MJ, Henkelman RM. T1, T2 relaxation and magnetization transfer in tissue at 3T. Magn Reson Med. 2005; 54:507–512. [PubMed: 16086319]
19. Tang Y, Yamashita Y, Takahashi M. Ultrafast T2-weighted imaging of the abdomen and pelvis: use of single shot fast spin-echo imaging. J Magn Reson Imaging. 1998; 8:384–390. [PubMed: 9562065]
20. Miyazaki M, Sugiura S, Tateishi F, Wada H, Kassai Y, Abe H. Non-contrast-enhanced MR angiography using 3D ECG-synchronized half-Fourier fast spin echo. J Magn Reson Imaging. 2000; 12:776–783. [PubMed: 11050650]
21. Lustig M, Pauly JM. SPIRiT: iterative self-consistent parallel imaging reconstruction from arbitrary k-space. Magn Reson Med. 2010; 64:457–471. [PubMed: 20665790]
22. Chen W, Meyer CH. Semiautomatic off-resonance correction in spiral imaging. Magn Reson Med. 2008; 59:1212–1219. [PubMed: 18429033]
23. Chen W, Sica CT, Meyer CH. Fast conjugate phase image reconstruction based on a Chebyshev approximation to correct for B0 field inhomogeneity and concomitant gradients. Magn Reson Med. 2008; 60:1104–1111. [PubMed: 18956462]
24. Ahn CB, Kim JH, Cho ZH. High-speed spiral-scan echo planar NMR imaging - I. IEEE Trans Med Imaging. 1986; 5:2–7. [PubMed: 18243976]
25. Meyer CH, Hu BS, Nishimura DG, Macovski A. Fast spiral coronary artery imaging. Magn Reson Med. 1992; 28:202–213. [PubMed: 1461123]

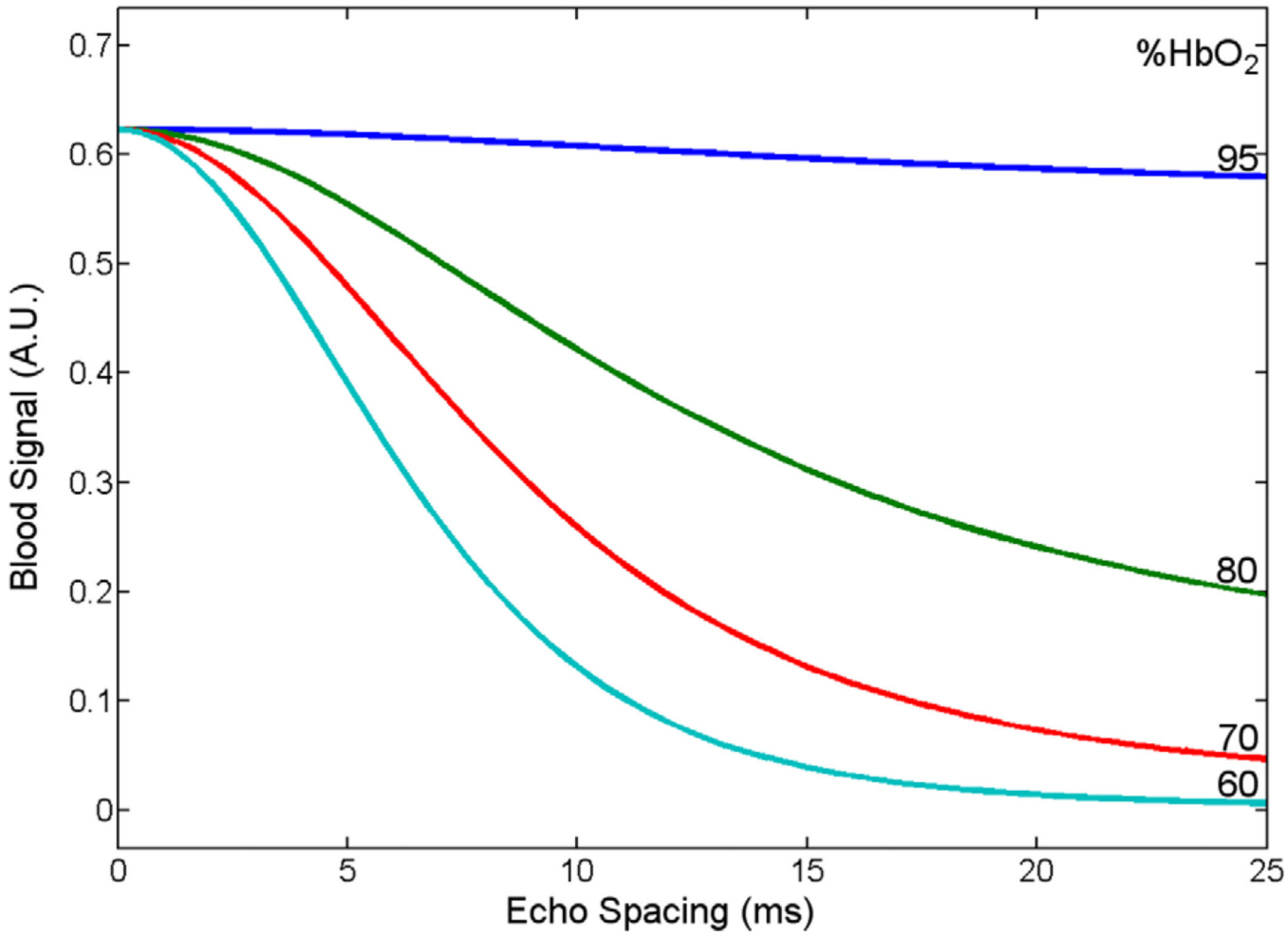

FIG. 1.

Blood signal at TE = 130 ms as a function of oxygenation state and echo spacing, using the Luz-Meiboom equation to estimate blood T_2 in a rapidly refocused sequence. For typical venous oxygenation values, much of the change in effective T_2 occurs as the echo spacing is increased from 0 to 10 ms. [Color figure can be viewed in the online issue, which is available at wileyonlinelibrary.com.]

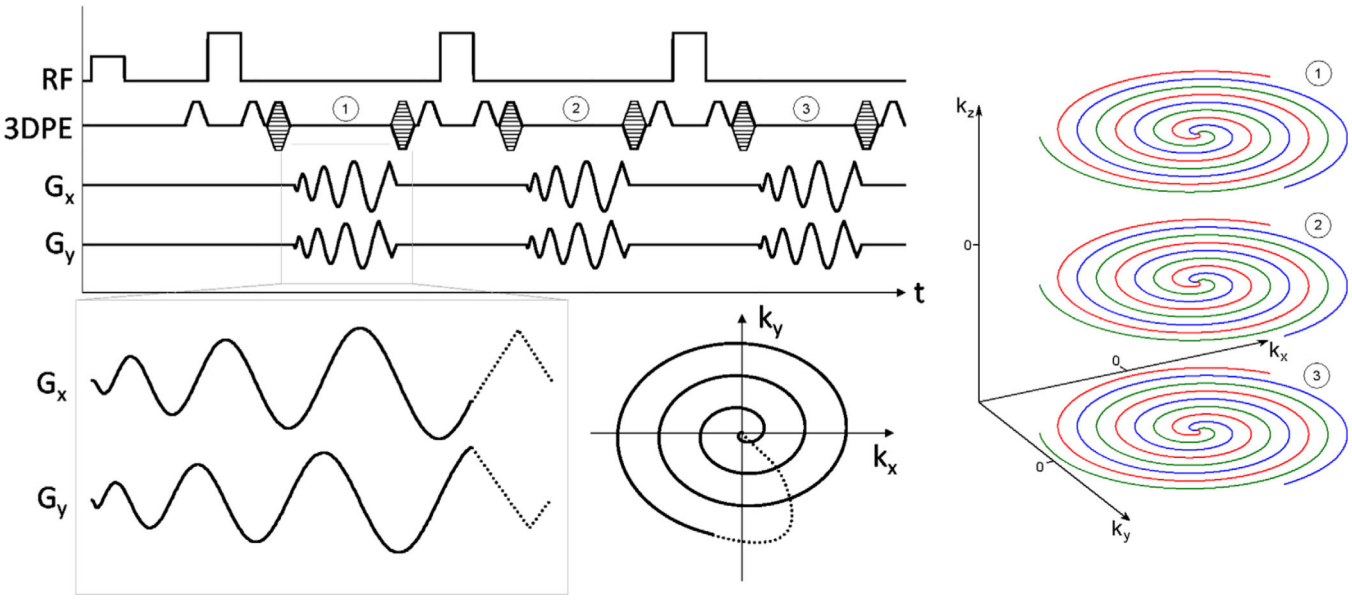

FIG. 2.

Spiral 3D TSE sequence diagram and resulting k-space trajectory. The same interleaf from each 3D phase encode is acquired in a single echo train. Partitions (3D phase encodes) are acquired linearly through the third k-space dimension and scrolled to achieve the desired TE. Echo train 1 acquires the red interleaf from partitions 1, 2, and 3, with partition 2 encoded as the center partition. After a wait time TR, echo train 2 acquires the green interleaf, and so on. Within each echo spacing, the net area of the readout gradients is zero.

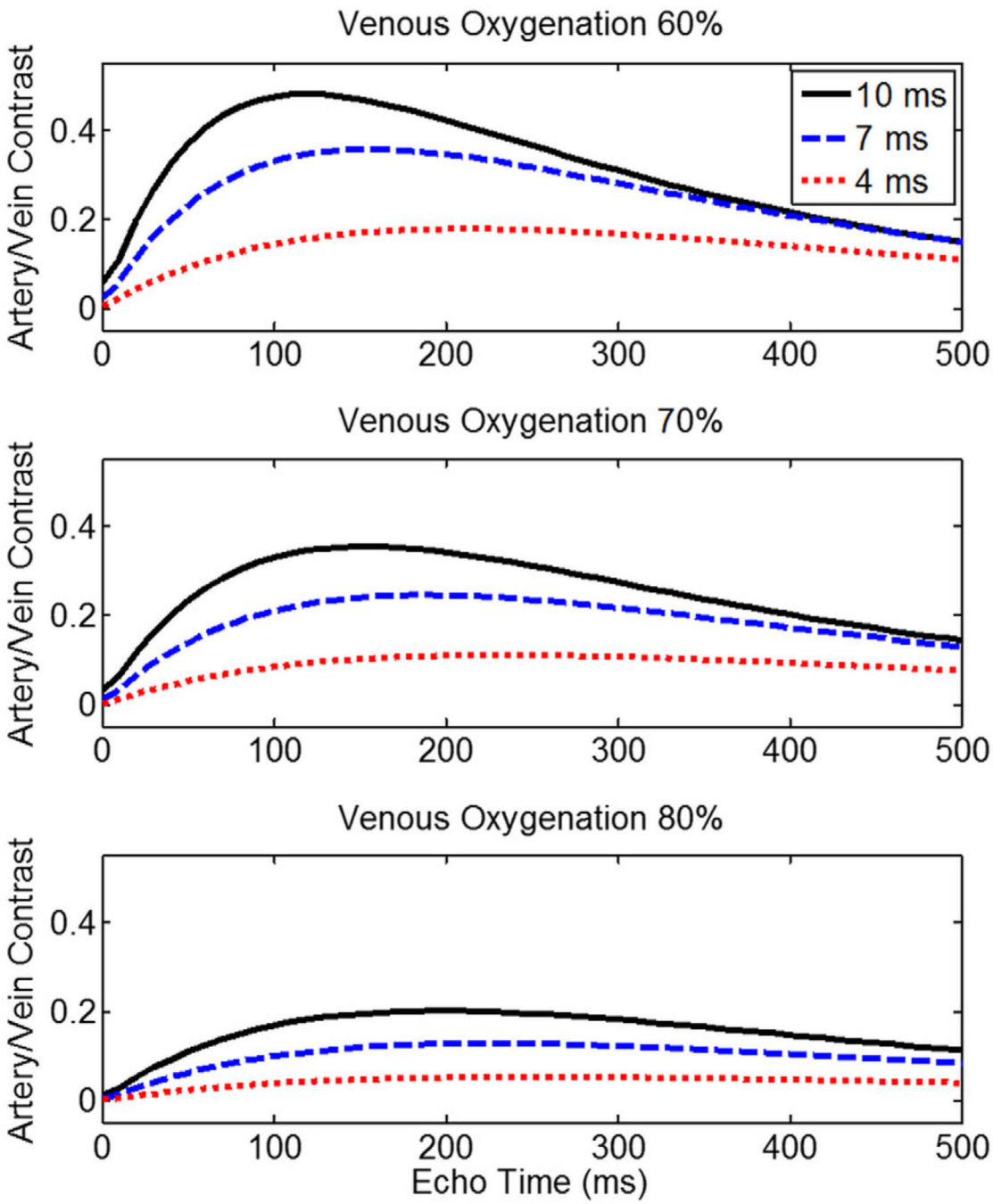

FIG. 3.

Artery–vein contrast as a function of echo time and venous oxygenation status during a TSE sequence. Maximum contrast occurs earlier and peaks at a higher level when longer echo spacings are used between refocusing RF pulses.

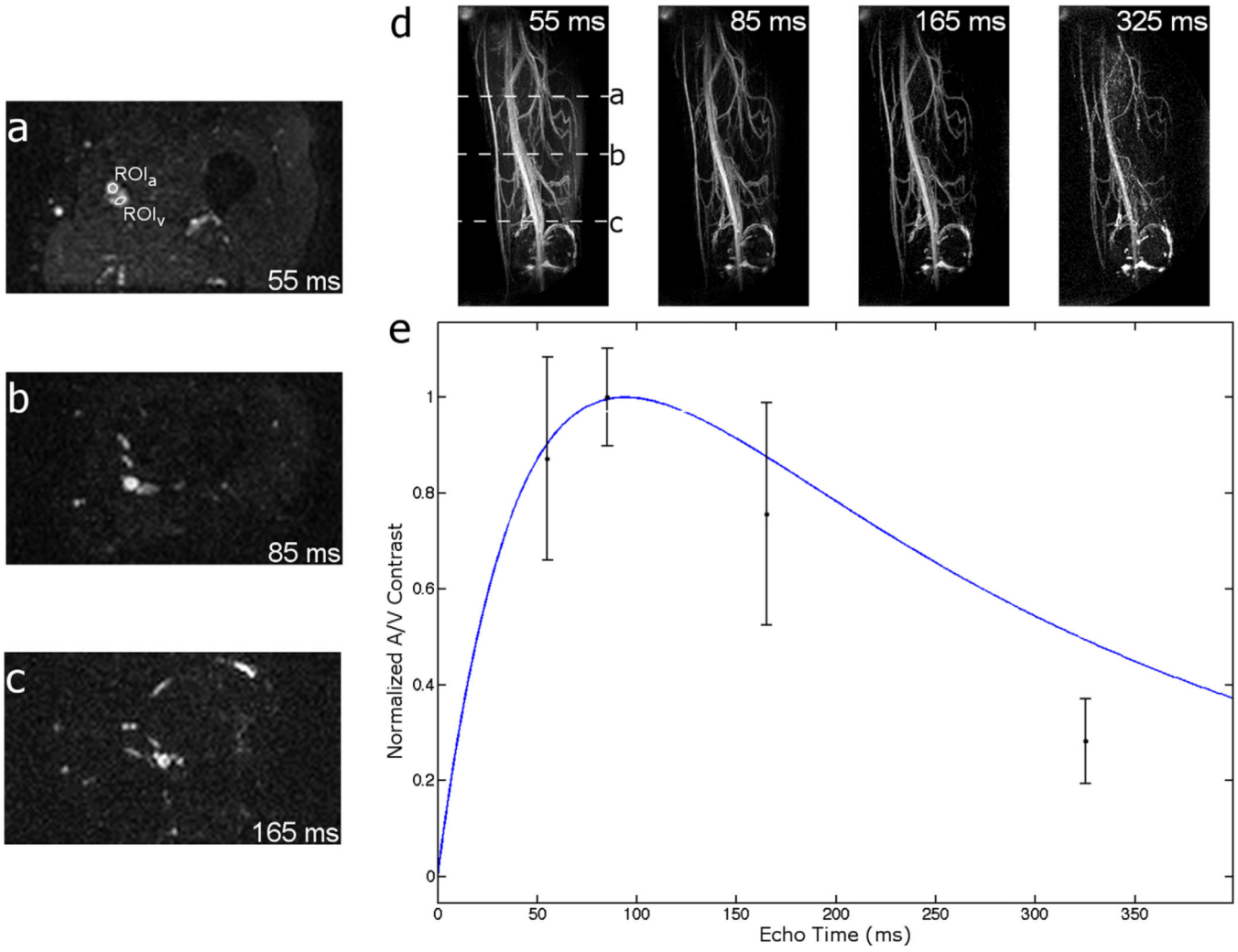

FIG. 4.

Spiral TSE noncontrast angiograms. **a–c:** Axial cross-sections of volumetric image data at TE = 55, 85, and 165 ms, respectively. Each axial slice's position is indicated in the 55 ms MIP image of (d). **d:** MIP images of a normal volunteer's thigh at various TEs. **e:** Plot of measured and predicted artery–vein contrast. Artery–vein contrast is maximized at TE just over 100 ms and follows the general shape predicted by Bloch equation simulations (see Fig. 3) of artery–vein contrast evolution (blue line). Muscle signal is suppressed with any choice of TE > 80 ms. [Color figure can be viewed in the online issue, which is available at wileyonlinelibrary.com.]

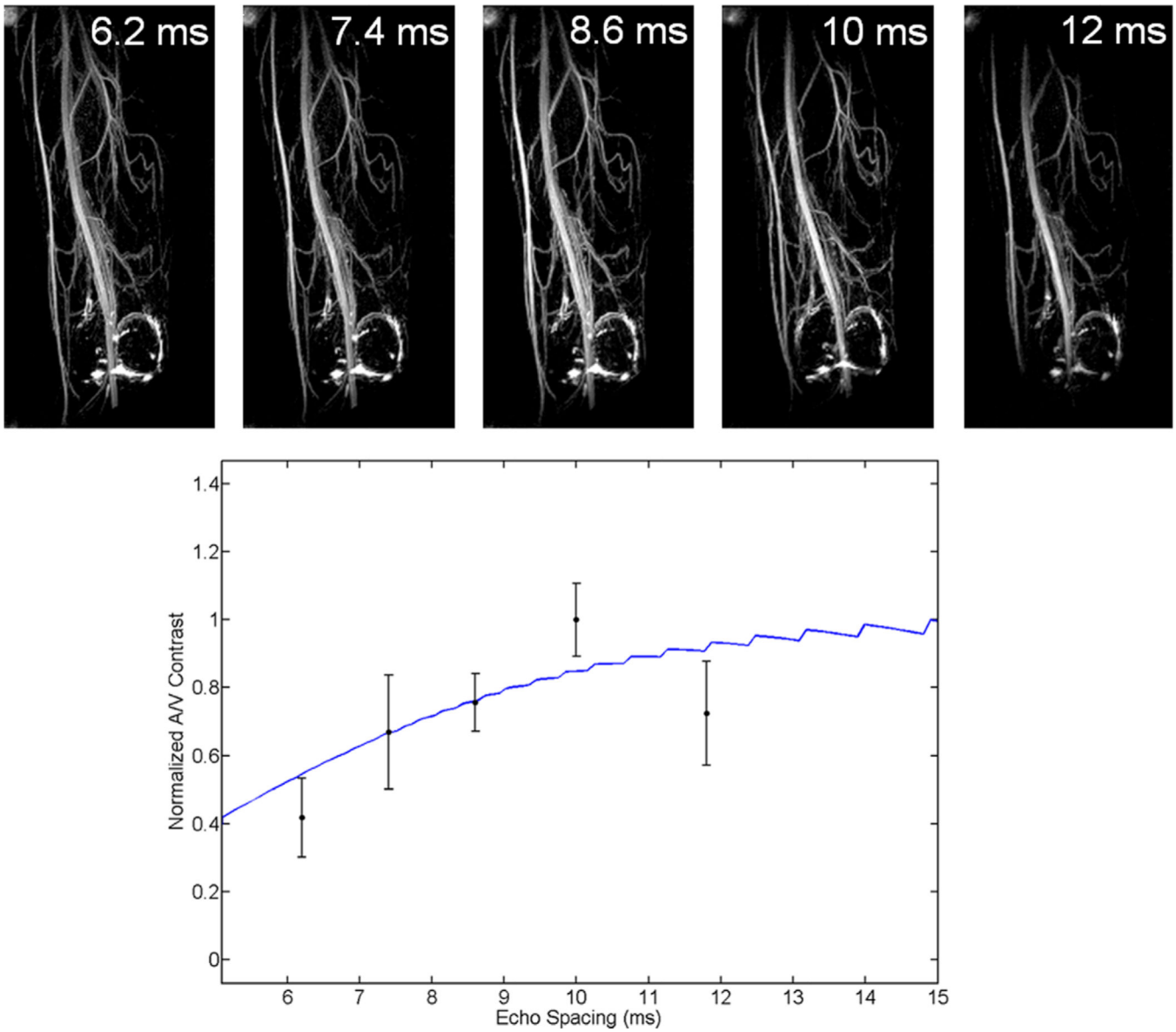

FIG. 5.

Top: MIP images of a normal volunteer's thigh with various echo spacings. Bottom: Plot of measured and predicted artery–vein contrast. Artery–vein contrast improves as echo spacings are lengthened; however, in this implementation, very large spacings result in image blurring due to off-resonance accrual because the readout duration is fixed to fill the available time. The blue line represents Bloch equation simulations of artery–vein contrast at various echo spacings. [Color figure can be viewed in the online issue, which is available at wileyonlinelibrary.com.]

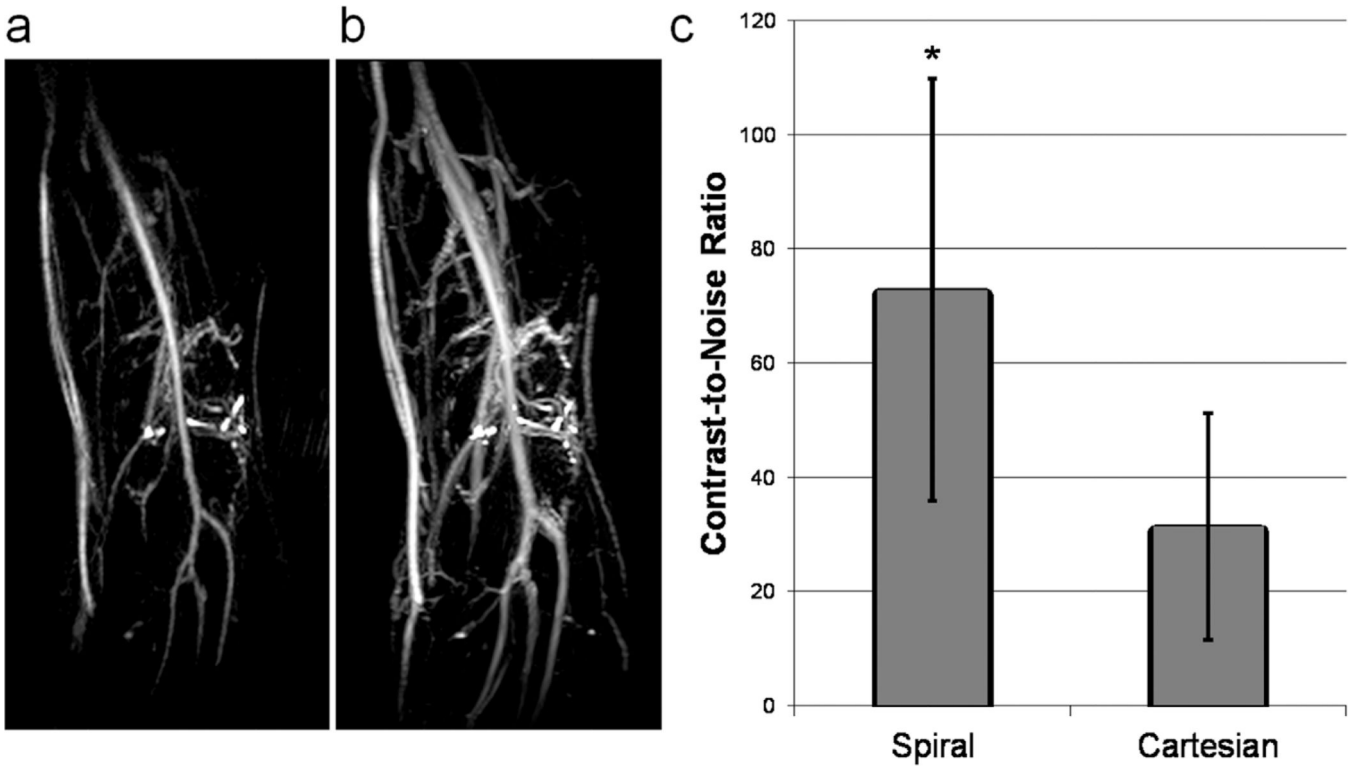

FIG. 6.

Spiral versus Cartesian TSE. **a:** Spiral TSE; echo spacing = 10 ms. **b:** Cartesian TSE; echo spacing = 3.8 ms. Confounding venous signal is observed in the Cartesian image and is nearly removed in the spiral image. Additionally, use of the spiral sequence results in better in-plane resolution. **c:** Quantification of artery/vein CNR based on three regions of interest placed in each of the femoral artery and vein. *$P < 0.05$.

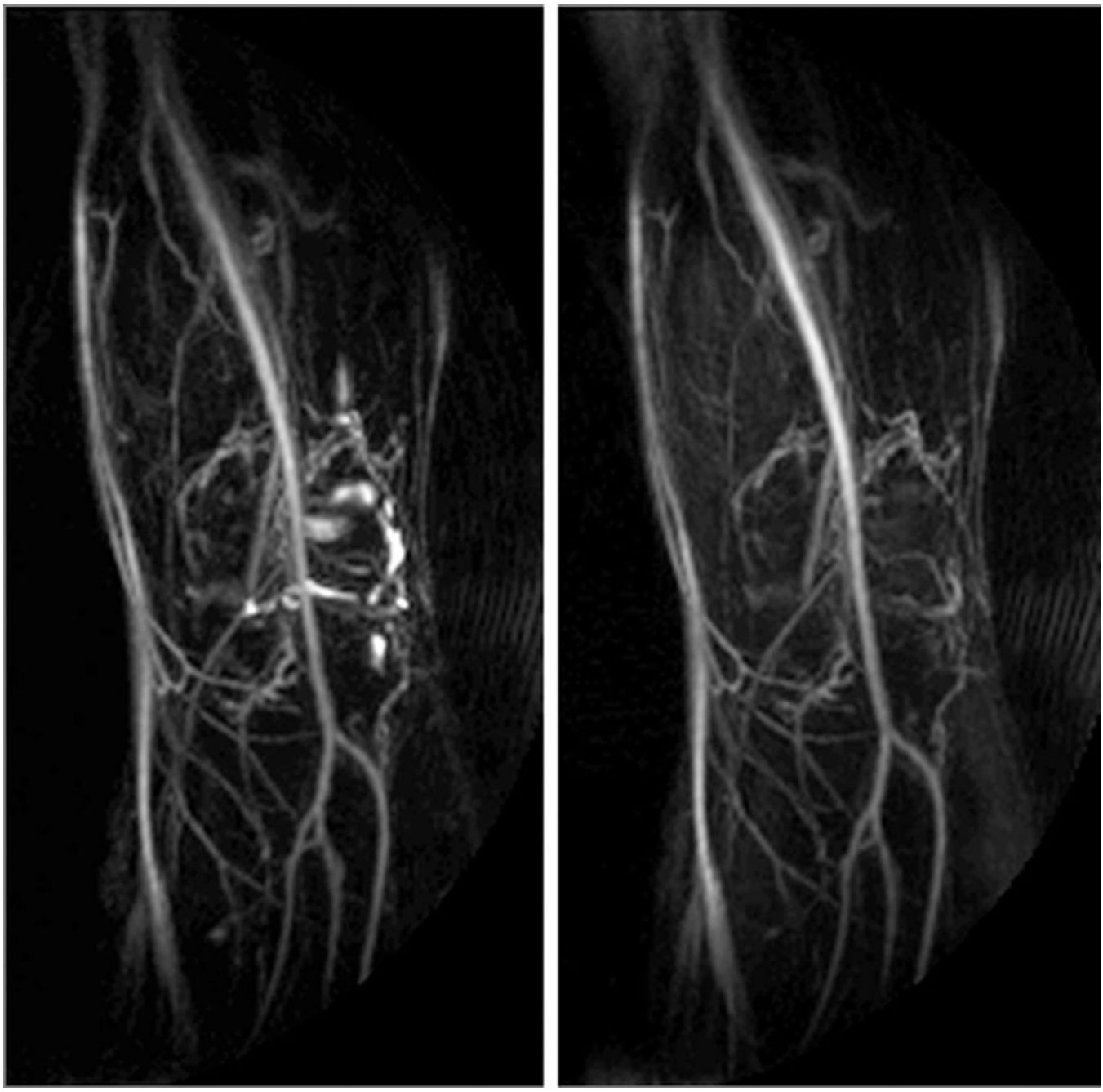

FIG. 7.

Left: No IR prep. Right: IR prep (FLAIR). Synovial fluid in the knee may be suppressed with the addition of an appropriately timed IR pulse, at the expense of signal and contrast.

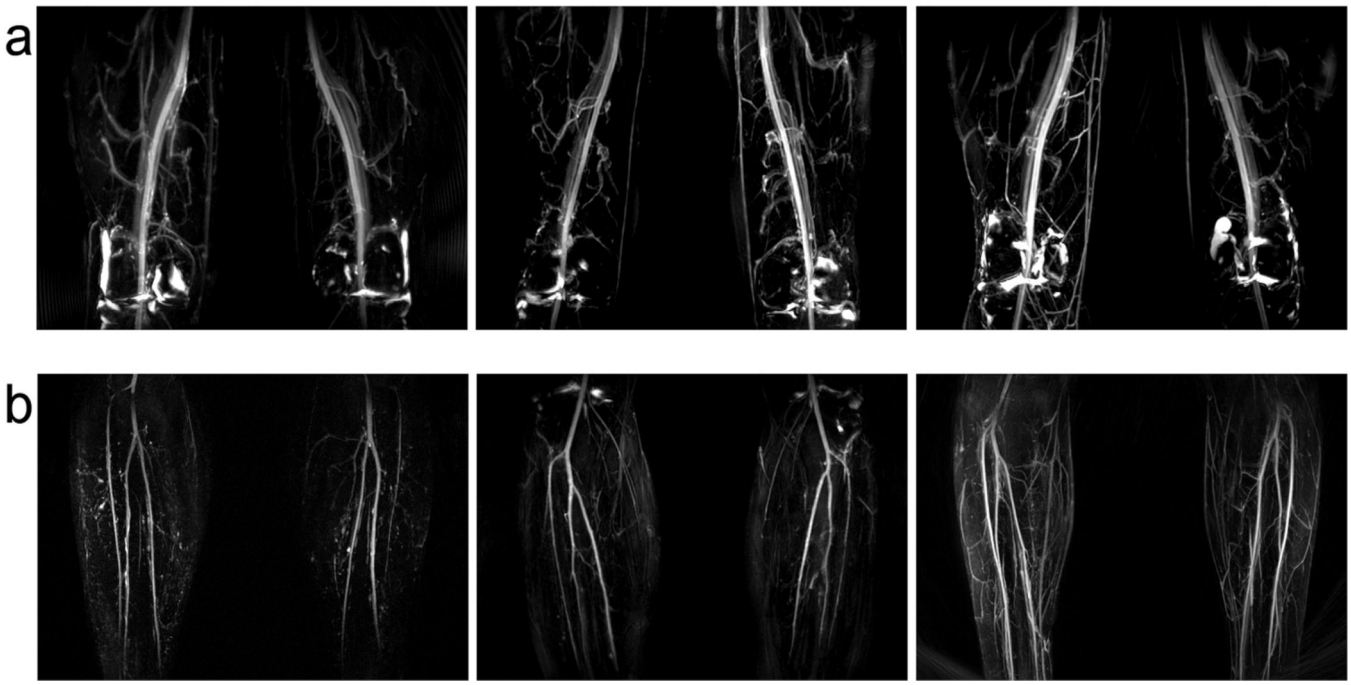

FIG. 8.

Volunteer data. All volunteers were scanned with the same protocol. **a:** Thigh station; synovial fluid is observed in the knee where a FLAIR pulse was not applied. **b:** Calf station; acquired with modest undersampling to improve resolution.